Published OnlineFirst May 6, 2020; DOI: 10.1158/1078-0432.CCR-19-2217

Phase II Trial of IL-12 Plasmid Transfection and PD-1 Blockade in Immunologically Quiescent Melanoma

Alain P. Algazi[1], Christopher G. Twitty[2], Katy K. Tsai[1], Mai Le[3], Robert Pierce[4], Erica Browning[2], Reneta Hermiz[2], David A. Canton[2], Donna Bannavong[2], Arielle Oglesby[1], Murray Francisco[2], Lawrence Fong[1], Mikael J. Pittet[5], Sean P. Arlauckas[6], Christopher Garris[7], Lauren P. Levine[1], Carlos Bifulco[8], Carmen Ballesteros-Merino[8], Shailender Bhatia[4], Sharron Gargosky[2], Robert H.I. Andtbacka[9], Bernard A. Fox[8], Michael D. Rosenblum[1], and Adil I. Daud[1]

ABSTRACT

Purpose: Tumors with low frequencies of checkpoint positive tumor-infiltrating lymphocytes (cpTIL) have a low likelihood of response to PD-1 blockade. We conducted a prospective multicenter phase II trial of intratumoral plasmid IL-12 (tavokinogene telseplasmid; "tavo") electroporation combined with pembrolizumab in patients with advanced melanoma with low frequencies of checkpoint positive cytotoxic lymphocytes (cpCTL).

Patients and Methods: Tavo was administered intratumorally days 1, 5, and 8 every 6 weeks while pembrolizumab (200 mg, i.v.) was administered every 3 weeks. The primary endpoint was objective response rate (ORR) by RECIST, secondary endpoints included duration of response, overall survival and progression-free survival. Toxicity was evaluated by the CTCAE v4. Extensive correlative analysis was done.

Results: The combination of tavo and pembrolizumab was well tolerated with adverse events similar to those previously reported with pembrolizumab alone. Patients had a 41% ORR ($n = 22$, RECIST 1.1) with 36% complete responses. Correlative analysis showed that the combination enhanced immune infiltration and sustained the IL-12/IFNγ feed-forward cycle, driving intratumoral cross-presenting dendritic cell subsets with increased TILs, emerging T cell receptor clones and, ultimately, systemic cellular immune responses.

Conclusions: The combination of tavo and pembrolizumab was associated with a higher than expected response rate in this poorly immunogenic population. No new or unexpected toxicities were observed. Correlative analysis showed T cell infiltration with enhanced immunity paralleling the clinical activity in low cpCTL tumors.

Introduction

Interleukin-12 (IL-12), a cytokine produced by activated innate immune cells such as macrophages and DCs (1), coordinates many facets of a productive immune response. It triggers T cell and NK cell activation (2), Th1 polarization of $CD4^+$ cells (3), reduces regulatory T cell (Treg) activity (4), and, by a positive feed-forward loop with IFN-γ, establishes an inflammatory environment (5–7). Recently, we have shown that IL-12 production by intratumoral DCs in response to IFN-γ in the tumor microenvironment is required for successful anti-PD-1 immunotherapy (8). While systemic IL-12 has limited clinical efficacy and significant toxicity in patients (9, 10), preclinical (11), and clinical data (12, 13) show that intratumoral IL-12 (tavokinogene telseplasmid; "tavo") leads to sustained local expression of IL-12 and can produce objective responses in both injected and uninjected tumors. This is observed even at distant sites, suggesting that intratumoral tavo electroporation (i.t.-tavo-EP) can induce productive immune responses systemically (12).

On the basis of these data, we hypothesized that i.t.-tavo-EP could increase immune infiltration in patients with nonimmune-infiltrated, or "cold," melanoma, making these tumors more responsive to the anti-PD-1 antibody pembrolizumab and yielding more frequent and sustained clinical responses. To this end, we conducted a phase II clinical trial of i.t.-tavo-EP and the anti-PD-1 antibody pembrolizumab in patients who are unlikely to respond to anti-PD-1 antibody monotherapy, as defined by an absence of intratumoral "exhausted" or checkpoint-positive cytotoxic lymphocytes (cpCTL) in the tumor microenvironment (14). In addition to clinical response data, we also interrogated clinical samples from study patients to investigate associated immunologic changes in the tumor microenvironment and periphery.

Patients and Methods

Trial design

This multi-center, phase II, open label, single-arm trial in individuals with a low frequency of tumor-infiltrating lymphocyte (TIL) melanoma was registered at cancer.gov as NCT02493361. The trial was conducted in accordance with International Conference on Harmonization guidelines for Good Clinical Practice and the Code

[1]University of California, San Francisco, San Francisco, California. [2]OncoSec Medical Incorporated, Pennington, New Jersey. [3]DR HOPE LLC, Seattle, Washington. [4]Fred Hutchinson Cancer Research Center, Seattle, Washington. [5]Massachusetts General Hospital and Harvard Medical School, Boston, Massachusetts. [6]Perelman School of Medicine at the University of Pennsylvania, Philadelphia, Pennsylvania. [7]Rockefeller University, New York, New York. [8]Earle A. Chiles Research Institute, Portland, Oregon. [9]Huntsman Cancer Institute, Salt Lake City, Utah.

Note: Supplementary data for this article are available at Clinical Cancer Research Online (http://clincancerres.aacrjournals.org/).

A.P. Algazi and C.G. Twitty contributed equally to this article.

Corresponding Author: Adil I. Daud, University of California, San Francisco, 1600 Divisadero Street, Rm A741, San Francisco, CA 94113. Phone: 415-353-7392; Fax: 415-885-3802; E-mail: Adil.daud@ucsf.edu

Clin Cancer Res 2020;XX:XX–XX

doi: 10.1158/1078-0432.CCR-19-2217

Published OnlineFirst May 6, 2020; DOI: 10.1158/1078-0432.CCR-19-2217

Translational Significance

Nonimmune infiltrated ("cold") tumors have low frequencies of intratumoral tumor-reactive, checkpoint positive cytotoxic lymphocytes (cpCTL) and they are not as responsive to checkpoint blockade as immune infiltrated ("hot") tumors. Forced expression of the inflammatory cytokine IL-12 in the tumor microenvironment increases intratumoral cpCTLs. We conducted a phase II trial in patients with nonimmune-infiltrated melanoma using a combination of plasmid IL-12 electroporation (tavokinogene telseplasmid) and the PD-1 antibody pembrolizumab. In this "cold" melanoma population, the combination productively altered the tumor microenvironment and was associated with encouraging clinical responses.

of Federal and guided by the ethical principles of the Belmont Report. The protocol was approved by each local Institutional Review Board. All patients provided written, informed consent at the time of screening.

Study population (NCT02493361)

Anti-PD1 antibody experienced and naïve adults (≥18 years old) with metastatic or unresectable melanoma with accessible lesions were eligible. We have previously described how the proportion of $CD8^+$ tumor-infiltrating lymphocytes (TIL) coexpressing the exhaustion markers CTLA-4^{hi} and PD-1^{hi}, termed partially exhausted CTLs (peCTL) or checkpoint-positive CTLs (cpCTLs), accurately predicts response to anti-PD-1 monotherapy in melanoma (14, 15). Melanoma tumors with $CD8^+$ TILs consisting of less than 20% cpCTL are unlikely to respond (5.9%; 1 of 17), whereas patients with greater than 30% cpCTL are highly likely to respond (77.8%; 14 of 18). A fresh tissue biopsy was collected at screening and the frequency of $CD8^+CD45^+$ TIL that were PD-1^{hi}CTLA-4^{hi} was determined using flow cytometric analysis as described previously (15). Predicted PD-1 nonresponders were identified on the basis of a low proportion (<25%) of checkpoint-positive cytotoxic lymphocytes (cpCTL) or an absence of TIL infiltration at baseline. Individuals on immunosuppressive medication and patients with uveal melanoma, active central nervous system metastases, carcinomatous meningitis, or active autoimmune disease requiring immunosuppressive agents were excluded.

Combination study treatment (i.t.-tavo-EP and pembrolizumab)

I.t.-tavo-EP (pIL12; Tavokinogene telseplasmid, tavo) was injected into tumors at $^1/_4$ tumor volume at a concentration of 0.5 mg/mL followed by *in vivo* electroporation of six pulses at field strengths (E+) of 1,500 V/cm and pulse width of 100 μs at 300-millisecond intervals (i.t.-tavo-EP). A minimum of 0.1 mL tavo was injected per lesion for lesions < 0.1 cm^3. Pembrolizumab was administered as a flat dose of 200 mg i.v.

Treatment schedule

Individuals initiated the first cycle of i.t.-tavo-EP concurrently with the first injection of pembrolizumab, receiving both on day 1 of the first cycle. Pembrolizumab was administered on day 1 of each 3-week cycle. I.t.-tavo-EP was administered on days 1, 5, and 8 of every odd cycle (every 6 weeks; cycles 1, 3, 5, 7, etc.).

Duration of therapy

Treatment was continued for up to 2 years if individuals had stable disease or better and continued to benefit from treatment. Patients with unconfirmed disease progression were permitted to continue on treatment until disease progression was confirmed. Treatment with i.t.-tavo-EP was discontinued if there was regression of all superficial, accessible lesions, in which case patients continued with pembrolizumab monotherapy for up to 2 years.

Efficacy assessments

Best overall response rate (BORR) was evaluated using RECIST v1.1 and clinical assessment by investigator evaluation at each restaging assessment performed every 12 weeks (**Fig. 1**, rBOR and **Fig. 2** RECIST). Duration of response (DOR), progression-free survival, overall survival, and overall objective response rate evaluated by RECIST was also assessed. In addition to scoring responses by RECIST v1.1, we also scored responses by investigator clinical assessment, which was defined as ≥50% decrease in the sum of bidimensional measurements of all measured lesions, and latent responses compared to baseline (after RECIST progression or pseudoprogression) were included (**Fig. 1**, cBOR and **Fig. 2**, clinical assessment).

Safety assessments

Safety was assessed during the study by documentation of adverse events (AE) according to CTCAE 4.0.

Duration of follow-up

After the end of treatment, individuals were followed for 30 days for adverse event monitoring (90 days for serious adverse events). For subjects who discontinued for reasons other than progressive disease, every attempt was made to continue monitoring their disease status using radiologic imaging. Monitoring was continued until the start of a new anticancer treatment, documented disease progression, or death, whichever occurred first. Radiographic imaging in follow-up was performed as clinically indicated or per local standard of care. Individuals were followed for overall survival until death, withdrawal of consent, or the end of the study, whichever occurred first.

Immunologic assessments

Tumor tissue collection (formalin)

Tumor tissue procured by core-needle or punch biopsy was fixed in formalin-filled containers for 24–48 hours before being transferred into PBS. One biopsy per tissue container was stored at 4°C until shipped to Cureline Inc. for further processing. Specimens were embedded in paraffin and 8 × 10 μm tissue curls were cut by Cureline Inc. and shipped to OncoSec Medical. Upon delivery, tissue curls were stored at −80°C until RNA extraction.

PFPE/formalin-fixed paraffin-embedded tissue RNA isolation

Paraffin was removed from FFPE/formalin-fixed paraffin-embedded (FFPE) tissue curls prior to RNA isolation using the protocol in RecoverAll Total Nucleic Acid Kit (catalog no. AM1975). Tissue curls were treated with xylene and heated at 50°C for (3) minutes. After xylene incubation, an equal part of ethanol was added then spun down. Pellet was then resuspended in ethanol twice to wash. After centrifugation, ethanol was allowed to evaporate at 37°C. Following paraffin removal, the RNA was isolated following the RecoverAll protocol. Briefly, proteinase k was incubated with the

Published OnlineFirst May 6, 2020; DOI: 10.1158/1078-0432.CCR-19-2217

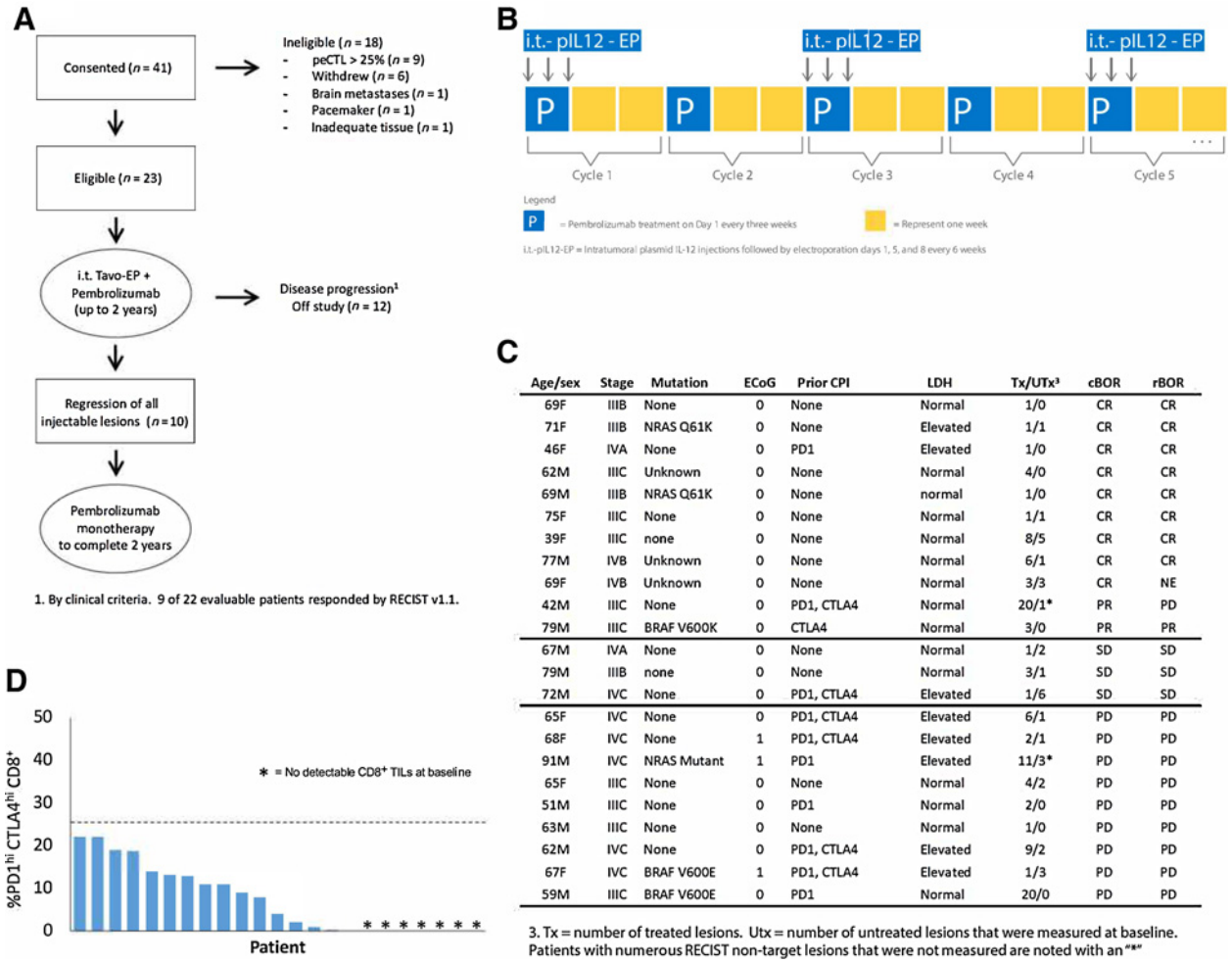

Age/sex	Stage	Mutation	ECoG	Prior CPI	LDH	Tx/UTx[3]	cBOR	rBOR
69F	IIIB	None	0	None	Normal	1/0	CR	CR
71F	IIIB	NRAS Q61K	0	None	Elevated	1/1	CR	CR
46F	IVA	None	0	PD1	Elevated	1/0	CR	CR
62M	IIIC	Unknown	0	None	Normal	4/0	CR	CR
69M	IIIB	NRAS Q61K	0	None	normal	1/0	CR	CR
75F	IIIC	None	0	None	Normal	1/1	CR	CR
39F	IIIC	none	0	None	Normal	8/5	CR	CR
77M	IVB	Unknown	0	None	Normal	6/1	CR	CR
69F	IVB	Unknown	0	None	Normal	3/3	CR	NE
42M	IIIC	None	0	PD1, CTLA4	Normal	20/1*	PR	PD
79M	IIIC	BRAF V600K	0	CTLA4	Normal	3/0	PR	PR
67M	IVA	None	0	None	Normal	1/2	SD	SD
79M	IIIB	none	0	None	Normal	3/1	SD	SD
72M	IVC	None	0	PD1, CTLA4	Elevated	1/6	SD	SD
65F	IVC	None	0	PD1, CTLA4	Elevated	6/1	PD	PD
68F	IVC	None	1	PD1, CTLA4	Elevated	2/1	PD	PD
91M	IVC	NRAS Mutant	1	PD1	Elevated	11/3*	PD	PD
65F	IIIC	None	0	None	Normal	4/2	PD	PD
51M	IIIC	None	0	PD1	Normal	2/0	PD	PD
63M	IIIC	None	0	None	Normal	1/0	PD	PD
62M	IVC	None	0	PD1, CTLA4	Elevated	9/2	PD	PD
67F	IVC	BRAF V600E	1	PD1, CTLA4	Elevated	1/3	PD	PD
59M	IIIC	BRAF V600E	0	PD1	Normal	20/0	PD	PD

3. Tx = number of treated lesions. Utx = number of untreated lesions that were measured at baseline. Patients with numerous RECIST non-target lesions that were not measured are noted with an "*"

Figure 1.

A, Study consort diagram. **B,** Combination study schema. **C,** Patient demographics ($n = 22$) at baseline and study schema for combination therapy including prior treatment for each patient and subsequent responses to i.t.-tavo-EP with pembrolizumab on this study. **D,** Intratumoral $CD8^+$ TILs from included patients were < 25% cpCTL (PD-1hiCTLA-4hi).

resuspended pellet for 1 hour at 55°C. After incubation, the solution was transferred into a PureLink spin column with Isolation Additive and flow through was used in further steps for RNA isolation. Samples were washed twice and then DNase was added to the column for 15–30 minutes. An additional three washes were performed prior to addition of elution buffer. RNA was collected from the spin column following a 1-minute incubation and the elution step was repeated with fresh buffer. Samples were measured on a NanoDrop 2000c spectrophotometer to test for purity and concentration. RNA was stored at −80°C until use.

Blood collection (sodium heparin vacutainer)

Approximately 60 mL of venous blood was collected in sodium heparin vacutainer tubes (BD Biosciences, catalog no. 367874) and shipped overnight from the clinical site to OncoSec Medical at ambient temperature. Heparin tubes were immediately processed for peripheral blood mononuclear cells (PBMC) using standard Ficoll-Pacque (GE) gradient extraction as described previously (1). PBMCs were frozen in CryoStor 10 (BioLife Solutions) and stored in liquid nitrogen until use.

Blood collection (vacutainer CPT)

Approximately 60 mL of venous blood was collected in BD Vacutainer CPT tubes (BD Biosciences, catalog no. 367874) and spun at 1,500 to 1,800 RCF for at least 15 minutes within 2 hours of blood collection. Spun tubes were then shipped overnight from the clinical site to OncoSec Medical at ambient temperature. The top portion of the tubes was removed and washed twice in DPBS (Gibco) and PBMCs frozen in CryoStor 10 (BioLife Solutions) and stored in liquid nitrogen until use.

Blood collection (PAXgene DNA)

Approximately 8.5 mL of veinous blood was collected in PAXgene DNA tubes (PreAnalytix) and shipped overnight from the clinical site to OncoSec Medical at ambient temperature. Samples were then allowed to cool to 4°C before storage at −80°C.

NanoString nCounter

Total RNA was used with the nCounter system, according to the manufacturer's protocol (NanoString Technologies). In brief, 100 ng of total RNA was hybridized at 96°C overnight with the nCounter

Published OnlineFirst May 6, 2020; DOI: 10.1158/1078-0432.CCR-19-2217

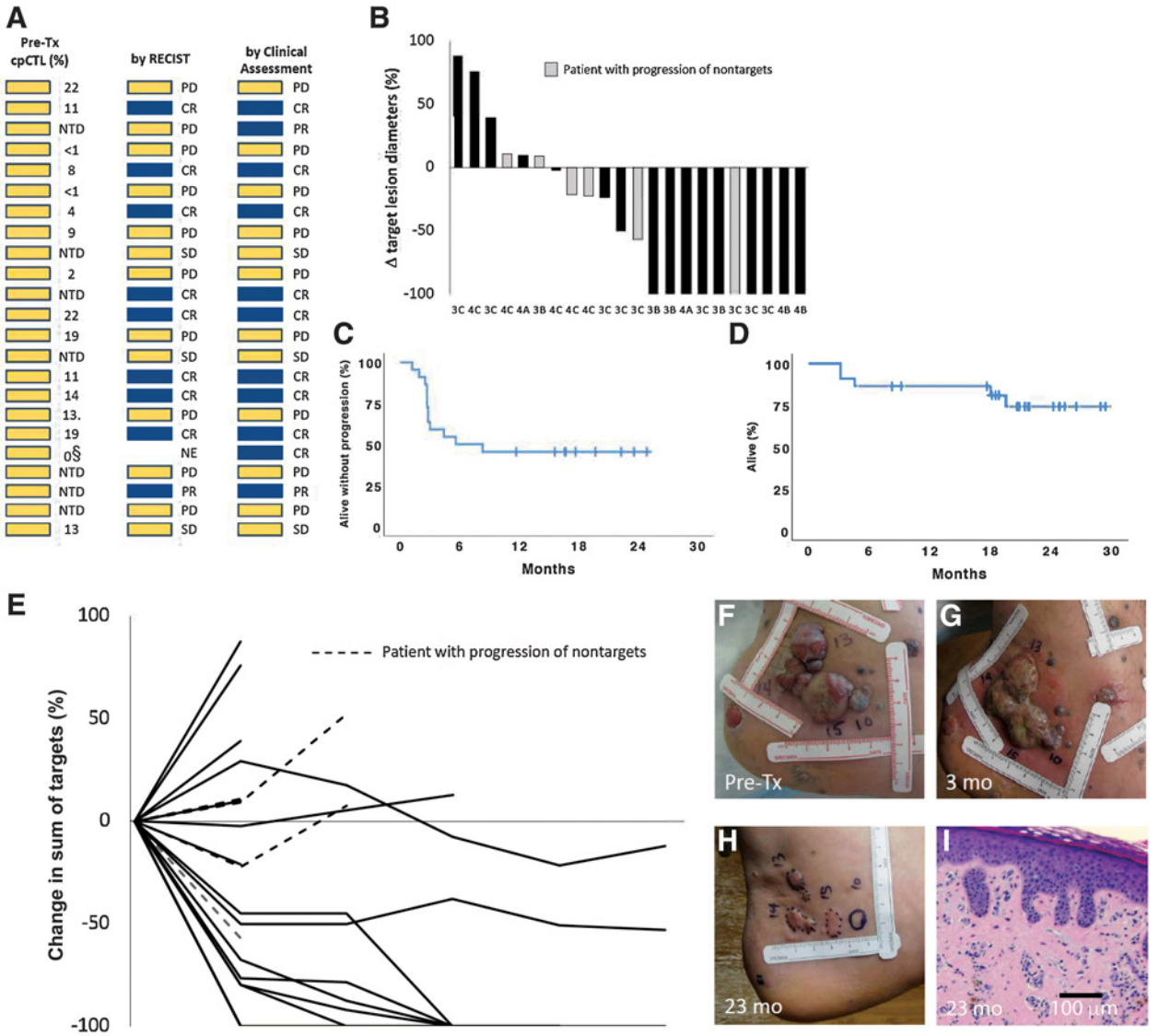

Figure 2.

A, Predicted responses and peCTL frequencies by the flow cytometry assay as well as the best observed clinical and RECIST v1.1 responses for each patient (blue, response; yellow, nonresponse). **B,** Waterfall plot of best response by clinical assessment. Clinical stage depicted on each bar progression-free survival (**C**) and overall survival (**D**) were determined using the Kaplan–Meier method. The median PFS was 5.6 months but the median OS was not reached at a median follow-up of 20.1 months. **E,** Individual patient RECIST responses over time (dashed lines represent patients with progression of nontarget lesions). **F–I,** A nonresponding anti-CTLA-4, anti-PD1 antibody refractory patient had a flare (**F–G**) of multiple unresectable in transit lesions followed by (**H**) an objective clinical response. **I,** A biopsy at 23 month shows only a siderotic scar with no residual melanoma. §, Patient did not have RECIST measurable disease at baseline.

(Human Immunology v2 Gene Expression Panels). This panel profiles approximately 600 immunology-related human genes as well as internal controls. Hybridized samples were then digitally analyzed for frequency of each RNA species using the nCounter SPRINT profiler. Raw mRNA abundance frequencies were quantified using the nSolver analysis software 3.0 pack. Data was normalized to control genes. Data were excluded if binding density, positive controls, or normalization factors were outside of the acceptable ranges set by NanoString.

Gene expression analysis

Normalized counts of RNA transcripts from patient biopsies were determined and expression was reported as relative to the average pre-treatment counts. These values were graphed in GraphPad Prism 7.03 and statistical analysis was determined as detailed in the statistical section below.

TCR-β sequencing

FFPE Tissue DNA Isolation: Paraffin was removed from PFPE tissue curls prior to DNA isolation. Tissue curls were treated twice with xylene. After last xylene incubation, equal parts of ethanol were added then spun down. The pellet was then resuspended in ethanol to wash. After centrifugation, ethanol was allowed to evaporate for 5 minutes at 37°C. Following paraffin removal, the protocol in Qiagen PAXgene Tissue AllPrep DNA/RNA/miRNA Kit (Venlo, catalog no. 80224) was

Published OnlineFirst May 6, 2020; DOI: 10.1158/1078-0432.CCR-19-2217

followed. Briefly, proteinase k was incubated with the resuspended pellet, shaking, for 2 hours at 45°C. After incubation, the solution was transferred into a PAXgene DNA spin column and washed once. An additional proteinase K incubation occurred on the spin column, followed by a wash and drying of the column membrane. Resuspension buffer containing DNA was collected from the spin column following a 5-minute incubation and measured on a NanoDrop 2000c spectrophotometer to test for purity and concentration. DNA was stored at −80°C until use.

Genomic DNA isolation from PBMC

Genomic DNA (gDNA) was isolated using the spin protocol in Qiagen's DNeasy Blood and Tissue Kit (Venlo, catalog no. 69504) using no more than 5×10^6 cells per column. Briefly, previously separated and frozen PBMCs were thawed and incubated with proteinase K for 10 minutes at 56°C, after which ethanol was added. The entire sample was transferred to a DNeasy spin column and washed twice. Resuspension buffer was run through the column twice before resuspended DNA was measured on a NanoDrop 2000c spectrophotometer to test for purity and concentration. Samples were stored at −80°C until use.

Adaptive analysis

Data was made available through the immunoSEQ Analyzer (Adaptive Biotechnologies). Differential abundance was calculated with 99% confidence through immunoSEQ to determine the number of clones differentially expressed between patient samples at screening and posttreatment.

Flow cytometry

PBMCs isolated as previously described from blood samples obtained from patients were analyzed for immune cell subsets by flow cytometry. Frozen PBMCs were thawed quickly by the addition of warm (37°C) X-Vivo 15 culture media (Lonza, catalog no. 04-418Q) containing IL-2 at 1,000 CU/mL (6,000 IU/mL). Cells were rested overnight at 37°C in humid conditions and 5% CO_2 as needed. Cells were stained for viability using BD HorizonTM Fixable Viability Stain 780 for 30 minutes at 4°C. Cells were stained for surface markers by incubating in the presence of fluorescence-conjugated antibody (Supplementary Table S1) below) for 30 minutes at 4°C. Intracellular staining was carried out by first incubating cells in 1× transcription factor fixation/permeabilization solution (BD Biosciences, catalog no. 562574) according to the manufacturer's protocol to fix and permeabilize the cells. Antibodies for intracellular staining were then added to cells. After a 45-minute incubation at 4°C, cells were washed, resuspended in FACS buffer and acquired on an LSRFortessa X-20 flow cytometer (BD Biosciences).

IHC

Multispectral IHC

Tissue sections were cut at 4 μm from FFPE blocks. All the sections were deparaffinized and subjected to heat-induced epitope retrieval in citrate buffer pH 9.0 (Biogenex). Six-plex panel IHC was performed for each tissue slide using the following antibodies: anti-FoxP3 (clone 236A/E7, dilution 1:100, Abcam), anti-PD-L1 (clone E1L3N, dilution 1:250, Cell Signaling Technology), anti-CD8 (clone SP16, dilution 1:50, Spring Bioscience), anti-CD3 (clone SP7, dilution 1:50, Spring Bioscience), anti-CD163 (clone MRQ26, Ventana), anti-Cytokeratin (clone AE1/AE3, dilution 1:100, DAKO). Antigen–antibody binding was visualized with TSA-Cy5 (PerkinElmer), TSA-Cy3 (PerkinElmer), TSA-FITC (PerkinElmer), TSA-Alexa594, TSA-Cy5.5 (PerkinElmer), and TSA-Coumarin (PerkinElmer), respectively.

Digital images were captured with PerkinElmer Vectra platform. Tumor areas with the highest immune cell ($CD3^+CD8^+$) infiltrates were scanned at 20X and selected for analysis in a blinded fashion. Three images of 0.36-mm^2 each were analyzed per sample with InForm Software (PerkinElmer). Hematoxylin and eosin staining was performed on for each sample and reviewed by a pathologist to ensure a representative tissue sample.

Chromogenic IHC

Punch or core biopsies were taken from treated lesions up to two weeks before treatment and at different time points on therapy. Untreated biopsies were also taken after treatment. Biopsies were FFPE, and cut into 5-μm sections. These FFPE of PFPE sections were immunostained for CD8, clone 144B, (Dako, catalog no. M7103) using methods established by PhenoPath for use in clinical diagnostics and for PD-L1, clone 22C3, (Dako, catalog no. SK006) per kit instructions. Whole slide digital images were captured using Aperio imaging software. All slides were evaluated by a board-certified pathologist and blindly scored for PD-L1 on a scale of 0–5 per the melanoma scoring guidelines listed below. Hematoxylin and eosin (H&E) staining was also performed for morphologic assessment and tumor location. A score of 0 = no staining; 1 = 0% to < 1%; staining; 2 = 1% to < 10% staining; 3 = 10% to < 33% staining; 4 = 33% to < 66% staining; 5 = ≥ 66%.

Statistical analysis

The primary endpoint was best overall response rate (BORR), CR + PR as determined by RECIST v1.1. Progression-free survival (PFS) was defined as the duration between the date of the first date of treatment on study to the first date of either disease progression or death; Overall survival was defined as was defined as the duration between the date of first treatment to the time of death. Individuals with measurable disease at baseline, which was defined separately under investigator evaluation, who received at least one dose of i.t.-tavo-EP and pembrolizumab study treatment, were included in the full analysis set population (FAS).

Analysis was performed using the R language. Progression-free survival (PFS) and overall survival (OS) were estimated using the method of Kaplan–Meier. To obviate the need to make distributional assumptions, statistical significance was assessed using rank-based methods. In particular, the Mann–Whitney test was used to for unpaired analysis and the Wilcoxon signed rank test was used for paired analysis between pretreatment and posttreatment. Exact tests using the Wilcoxon. exact function in the package exact RankTests were performed due to small sample sizes. Tests with P values less than 0.05 were considered significantly significant. For the gene expression analysis depicted in **Fig. 4**, raw gene scores (NanoString Inc) were analyzed using a negative binomial generalized linear model with individual level random effect adjustment for pairing. The raw gene level P values were adjusted for multiple comparisons using the Benjamini–Hochberg method (**Fig. 4A**) or the Wilcoxon matched-pairs signed rank test (**Fig. 4B–D**).

Sample size and study hypothesis

This study was a single-arm combination study with a historical comparator, thus the sample size depended on the presumed "baseline pembrolizumab ORR" in the biomarker-selected population, as defined by the low TIL status (a cutoff of 25% cpCTLS was chosen in the study) on the screening flow cytometric assay measures. The

Published OnlineFirst May 6, 2020; DOI: 10.1158/1078-0432.CCR-19-2217

predicted response rate of patients in this population was estimated at 12.5% (based on RECIST1.1) based on analysis of melanoma patients at University of California, San Francisco treated with pembrolizumab as a monotherapy who had fewer than 25% cpCTLs prior to the initiation of treatment. We posited that ORR of >30% in patients treated with pIL-12 EP combined with pembrolizumab would be clinically meaningful. Therefore, inclusion of 42 individuals would meet the following statistical parameters: H_0 ORR = 12.5%; H_{alt} ORR = 30%; alpha of 0.025 (actual; one-sided test); power = 85%.

Interim safety and efficacy assessments were performed after 23 evaluable were enrolled. The interim results showed the ORR rate, 41% by RECIST (and 50% by clinical assessment) with 36% complete responses, far exceeded the projected response rate in the hypothesis. The investigators stopped accrual and a larger confirmatory trial was initiated.

Results

Selection of patients with immunologically "cold" tumors

A total of 41 patients were screened for this trial (study schema, **Fig. 1A** and study design **Fig. 1B**), and 23 patients, including 22 patients with RECIST measurable disease at baseline, were eligible to participate based on a $CD8^+$ cpCTL (or peCTL) percentage of less than 25% in tumor biopsy specimens taken at screening (**Fig. 1A**). We also examined the trial population with previously described PD-1 predictive biomarker assays including PD-L1 IHC using the 22C3 mAb (16) and IFNγ gene expression signatures (17). Tumors evaluated by either method had a low likelihood of response (**Fig. 2A**; Supplementary Fig. S1). Baseline patient characteristics are described in **Fig. 1C**. Of note, 10 patients had prior exposure to anti-PD-1 antibodies and 7 patients had prior exposure to anti-CTLA4 antibodies.

Clinical response and adverse event data on the i.t.-tavo-EP and pembrolizumab trial

The ORR was 48% (11/23) by clinical assessment (including 1 patient with RECIST nonmeasurable disease at baseline and 1 patient with a delayed response after progression) and 41% (9/22) by RECIST version 1.1 (**Fig. 2A** and **B**). Patients responses by RECIST and clinical criteria are shown in **Fig. 2A**. Responses were rapid and sustained (**Fig. 2E**). The median progression free survival by RECIST was 5.6 months (95% CI undefined). The median overall survival was not reached at a median follow up of 19.6 months. (**Fig. 2C** and **D**). These results are in contrast to those expected for predicted PD-1 nonresponders by the cpCTL assay (14). Objective responses were observed in patients with elevated LDH levels at baseline, prior exposure to anti-PD-1 antibodies, and in patients with stage IIIB to stage IVC disease (**Fig. 1C**). Clinical responses were observed in patients regardless of baseline TIL levels (**Fig. 2A**) or baseline PD-L1 protein levels by IHC (**Fig. 3B**). The median baseline interferon-γ expression signature of enrolled patients (Supplementary Fig. S1), 0.81, was > 1 SD below the mean reported for responders by Ayers and colleagues (17). Overall, 13 patients had untreated lesions measured at baseline and 10 of these patients had untreated RECIST target lesions at baseline. On a per lesion basis including both target and nontarget lesions (Supplementary Table S2), 29.2% of untreated lesions, including liver and lung metastases, decreased by > 30% in maximum diameter. The diameters of treated and untreated lesions were similar (mean = 2.6 ± 2.1 cm vs. 3.4 +/2.5 cm) as were the diameters of responding and progressing lesions (mean 3.4 ± 1.9 cm vs. 2.2 ± 2.1 cm). A patient with > 50 in-transit lesions at baseline and prior disease progression on ipilimumab, pembrolizumab, and nivolumab had a partial response after RECIST confirmed progression (**Fig. 2F–I**). In this patient, biopsied lesions posttreatment showed a siderotic scar with no evidence of residual melanoma by histopathology (**Fig. 2I**). In contrast to systemic IL-12 administration, the combination of tavo and pembrolizumab was well tolerated (Supplementary Table S3) and grade 3 or higher treatment associated toxicity was limited to treatment associated pain ($n = 1$), cellulitis ($n = 1$), chills ($n = 1$), and sweats ($n = 1$).

Tavo+pembro combination therapy increases TILs and adaptive resistance

The presence of tumor-infiltrating $CD8^+$ lymphocytes and high PD-L1 levels in the tumor microenvironment have been identified as dynamic predictors of response to PD-1 antibodies in patients with metastatic melanoma (18–20). The combination of i.t. tavo EP and pembrolizumab drove an increased density of $CD8^+$ TILs (**Fig. 3A**, $P = 0.027$) as well as a significant increase in the number of unique intratumoral T cell clones (**Fig. 5B**, $P = 0.041$). In addition, significant increases in intratumoral PD-L1 expression by IHC (**Fig. 3B**, $P = 0.016$), transcriptomic analysis (**Fig. 3C**, $P = 0.026$), and systemic proliferating PD-1^+ T cells (**Fig. 5D**, $P = 0.012$) were noted.

While multispectral IHC highlighted that i.t.-tavo-EP combination therapy can elicit an increase in adaptive tumoral and stromal PD-L1 expression in both responding and nonresponding patients (**Fig. 3D**), these groups differed in the relative balance of infiltrating immune subpopulations. In quantitative spatial analysis, nonresponding patients had more Tregs in close proximity to $CD8^+$ T cells than responding patients (**Fig. 3F**, $P = 0.018$). This balance of effector to suppressive immune subsets could also be seen in the positive ratio of $CD8^+$ T cells to M2 macrophages (PD-$L1^+$/$CD163^+$) in responding patients (**Fig. 3G**, $P = 0.011$).

Analysis of gene expression underlying productive immune responses

A critical hypothesis of this study was that IL-12 licenses the tumor immune environment by multiple mechanisms and increases the likelihood of effective anti-PD-1 therapy. Increased intratumoral transcription of an immune-based gene set following treatment was observed with i.t.-tavo-EP plus pembrolizumab (**Fig. 4A**). Effective anti-PD-1 therapy has also been shown to require the presence of cross-presenting cDC1 dendritic cells (20). In a pooled analysis of all patients at cycle 2 (week 3) of concurrent i.t.-tavo-EP + pembrolizumab, we found that cDC1-associated antigen presentation genes were also significantly increased intratumorally following combined treatment (**Fig. 4B**). In addition to antigen cross-presentation, expression of genes associated with T cell activation and adaptive resistance (**Fig. 4C**) as well as T cell trafficking and costimulation (**Fig. 4D**) was also significantly increased, similar to what Garris and colleagues recently reported (8). An increase in natural killer (NK) cell–associated genes was also noted (**Fig. 4B**). Transcriptome analysis highlighted treatment-related changes in relevant cell type scores, which were particularly evident when separated by clinical response (Supplementary Fig. S2).

IFN response factor-1 (IRF-1) is a transcription factor produced in response to IFNγ, linking stimuli to immune evasion via PD-L1 expression (21). Because the transcriptional analysis demonstrated that responding patients had a treatment-related increase in the expression of PD-L1 (**Fig. 3B** and **C**), we examined intratumoral

Published OnlineFirst May 6, 2020; DOI: 10.1158/1078-0432.CCR-19-2217

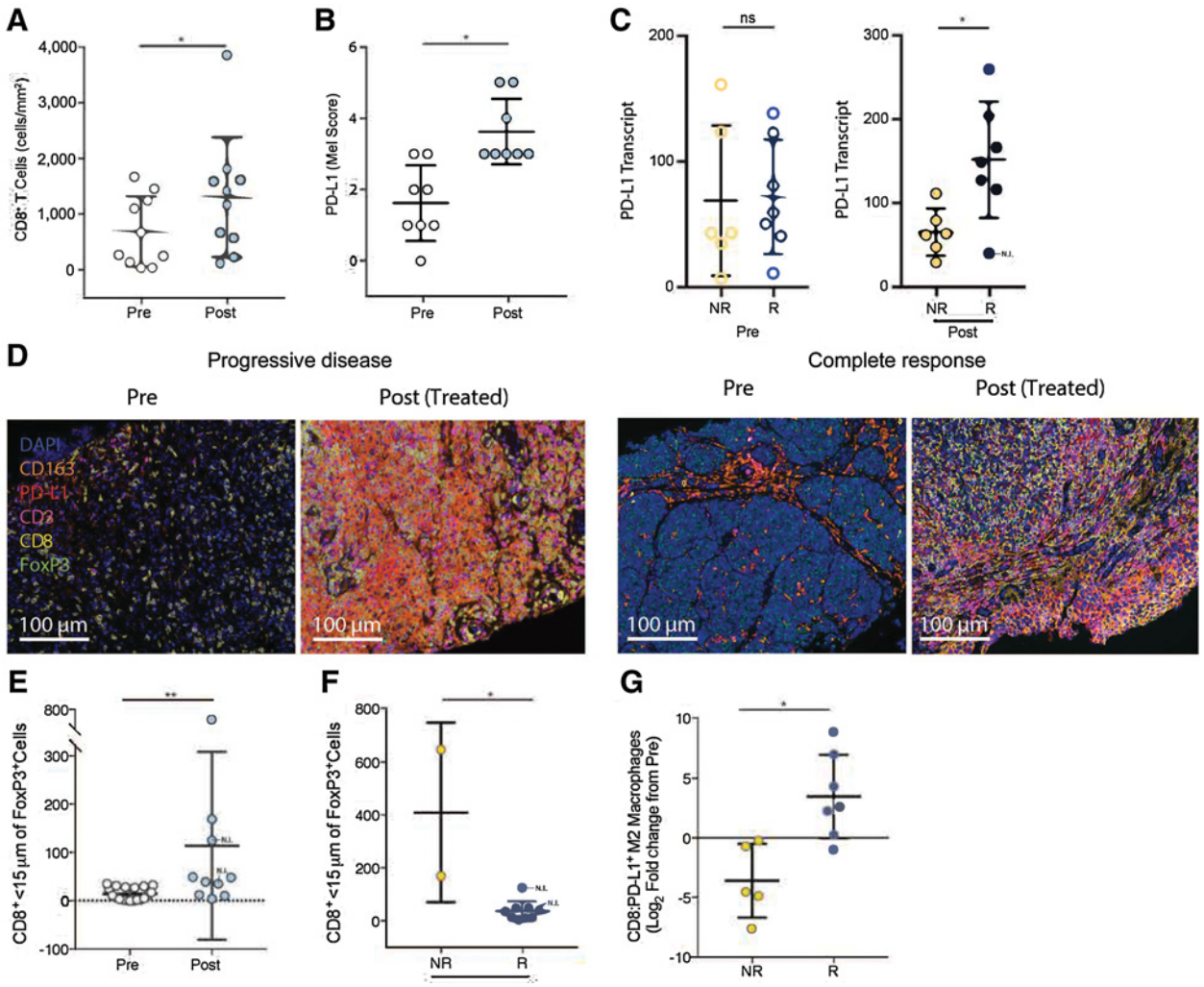

Figure 3.

Increasing TILs and adaptive resistance in i.t.-tavo-EP–treated lesions. FFPE tumor biopsies and PBMCs collected at pre- and posttreatment time points were stained for immune cell markers by multispectral mIHC and flow cytometry. **A,** An increase of intratumoral CD8$^+$ T cell density in FFPE biopsies of patients by mIHC analysis was observed after a single cycle of combination therapy. **B** and **C,** After a single cycle of intratumoral plasmid IL-12 with electroporation, intratumoral PD-L1 expression (**B**) measured by IHC was significantly increased while (**C**) transcriptional analysis demonstrated a significant posttreatment expression of PD-L1 in responding patients. **D,** mIHC images of a patient with progressive disease (left) shows increased CD163$^+$ TILs and PD-L1$^+$ cells whereas a patient undergoing a complete response (right) showed a brisk increase in CD8$^+$ TILs over one course of combination therapy. **E,** mIHC spatial analysis showed a significant increase in the number of FoxP3$^+$ cells < 15 µm from CD8$^+$ T cells in patients after a single cycle of combination treatment. **F,** Posttreatment, nonresponders showed a significantly higher amount of FoxP3$^+$ cells < 15 µm from CD8$^+$ T cells when compared with responders. **G,** Patients responding to combination treatment showed a significant increase in the ratio of CD8:M2 macrophages (CD163$^+$) after a single cycle of treatment. Pre, pretreatment; post, posttreatment, cycle 2 day 1; NR, nonresponder (stable disease and progressive disease); R, responder (complete response and partial response). Significance calculated by Mann–Whitney for all unpaired samples [**C** ($n = 6$ (NR), $n = 7$ (R)), **E** ($n = 18$ (pre), $n = 10$ (post), **F** ($n = 2$ (NR), $n = 9$ (R)) and g ($n = 5$ (NR), $n = 7$ (R))] and by Wilcoxon matched-pairs signed rank test for all paired samples [**A** ($n = 10$) and **B** ($n = 8$)]. ns, not significant; *, $P < 0.05$; **, $P < 0.01$; N.I., noninjected lesions were noted (**C**, **E**, and **F** only).

mRNA levels of IRF-1 and PD-L1 in i.t.-tavo-EP + pembrolizumab treated patients. As shown in **Fig. 5E** the correlation between IRF-1 and PD-L1 became significant with treatment, suggesting that the "capability" of tumor/immune cells to respond to IFNγ via IL-12 may factor into clinical response with this combination.

Distant responses and circulating immune cells suggest systemic immune responses

To understand how an intratumoral therapy can drive systemic immune responses, the architecture and context of immune infiltration in both electroporated and nonelectroporated tumors were examined by multispectral IHC (mIHC). As shown in a sample of nonresponding and responding patients (**Fig. 5A**), intense infiltration was seen at cycle 2 (week 3) in all interrogated lesions. This was the case in patients with progressive disease as well as in patients with objective responses. Regardless of electroporation, the composition of the infiltrate was a key determinate of clinical response as seen in the ratio of CD8$^+$ cells:M2 macrophages (**Fig. 5A**); similarly observed with the entire cohort (**Fig. 3G**). Additional support for combination therapy initiating systemic immunity beyond regression of

Published OnlineFirst May 6, 2020; DOI: 10.1158/1078-0432.CCR-19-2217

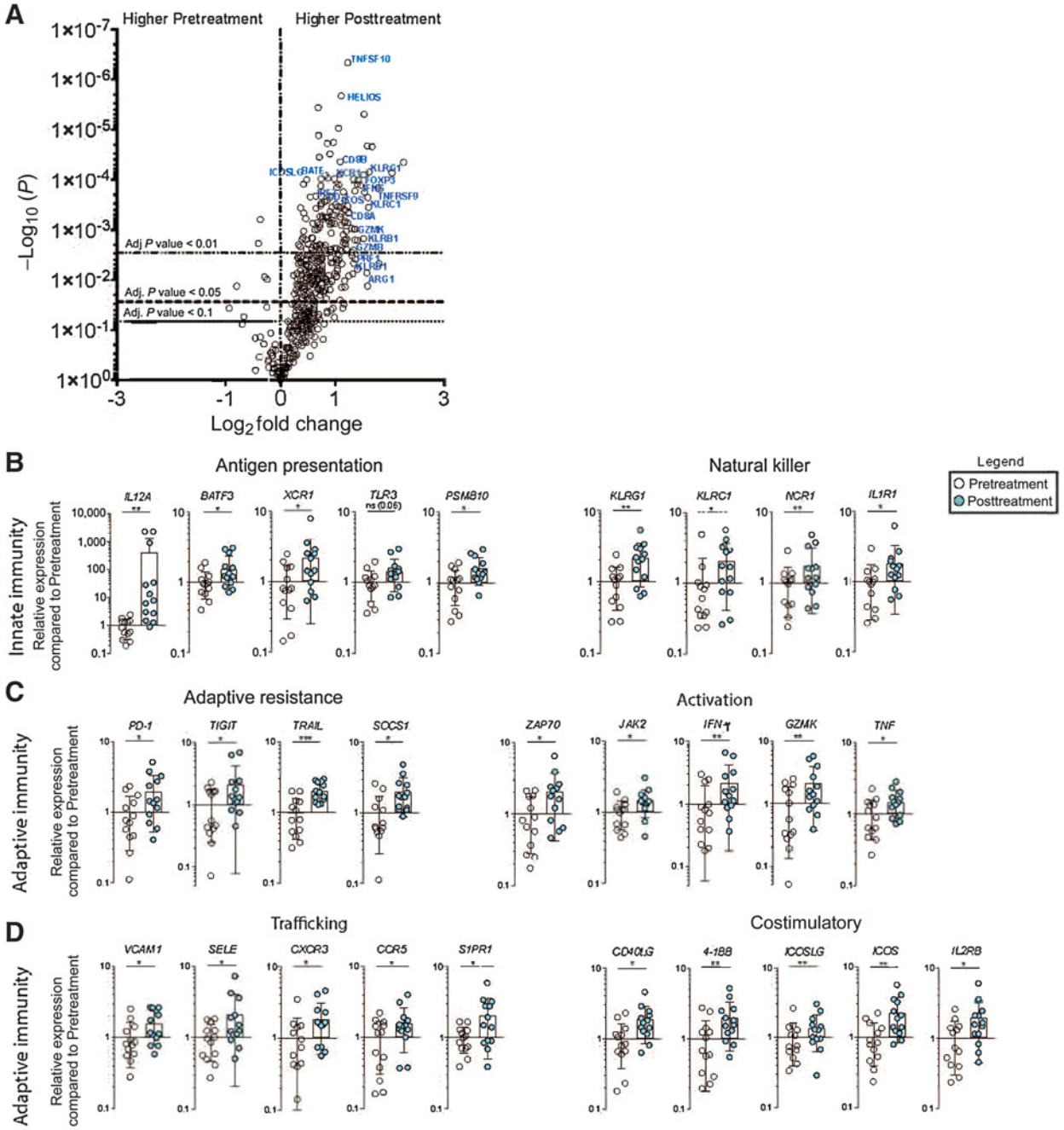

Figure 4.

Combination therapy enhances intratumoral expression of immune-based gene sets. Transcriptional analysis of biopsies collected at screen and post-treatment. **A,** Volcano plot of both nonresponding and responding patients highlight changes in Th1/antitumor-associated genes. On-treatment (after 1 cycle of treatment) increases in gene expression related to innate immunity (**B**), adaptive resistance and immune activation (**C**), immune trafficking and costimulation were noted in patients receiving combination therapy (**D**). Pre, pretreatment; post, posttreatment, (cycle 2 day 1). *, $P = 0.05$; **, $P = 0.01$; ***, $P = 0.001$ by Mann–Whitney t test ($n = 13$). Note, 1 untreated sample (after 1 cycle of treatment) was used in this analysis.

nonelectroporated lesions was evident in the treatment-related increase of activated immune cells measured in the periphery. In particular, combination of i.t.-tavo-EP and pembrolizumab resulted in a significant increase in proliferating T_{emra} cells in peripheral blood (**Fig. 5C**, $P = 0.008$).

Discussion

IL-12 is a pivotal type 1 immune regulatory cytokine (22, 23), which induces a positive feedback loop inducing T cells and NK cells to produce IFNγ that in turn primes DCs for IL-12 production (7). Despite its importance, effective strategies for increasing IL-12 in

Published OnlineFirst May 6, 2020; DOI: 10.1158/1078-0432.CCR-19-2217

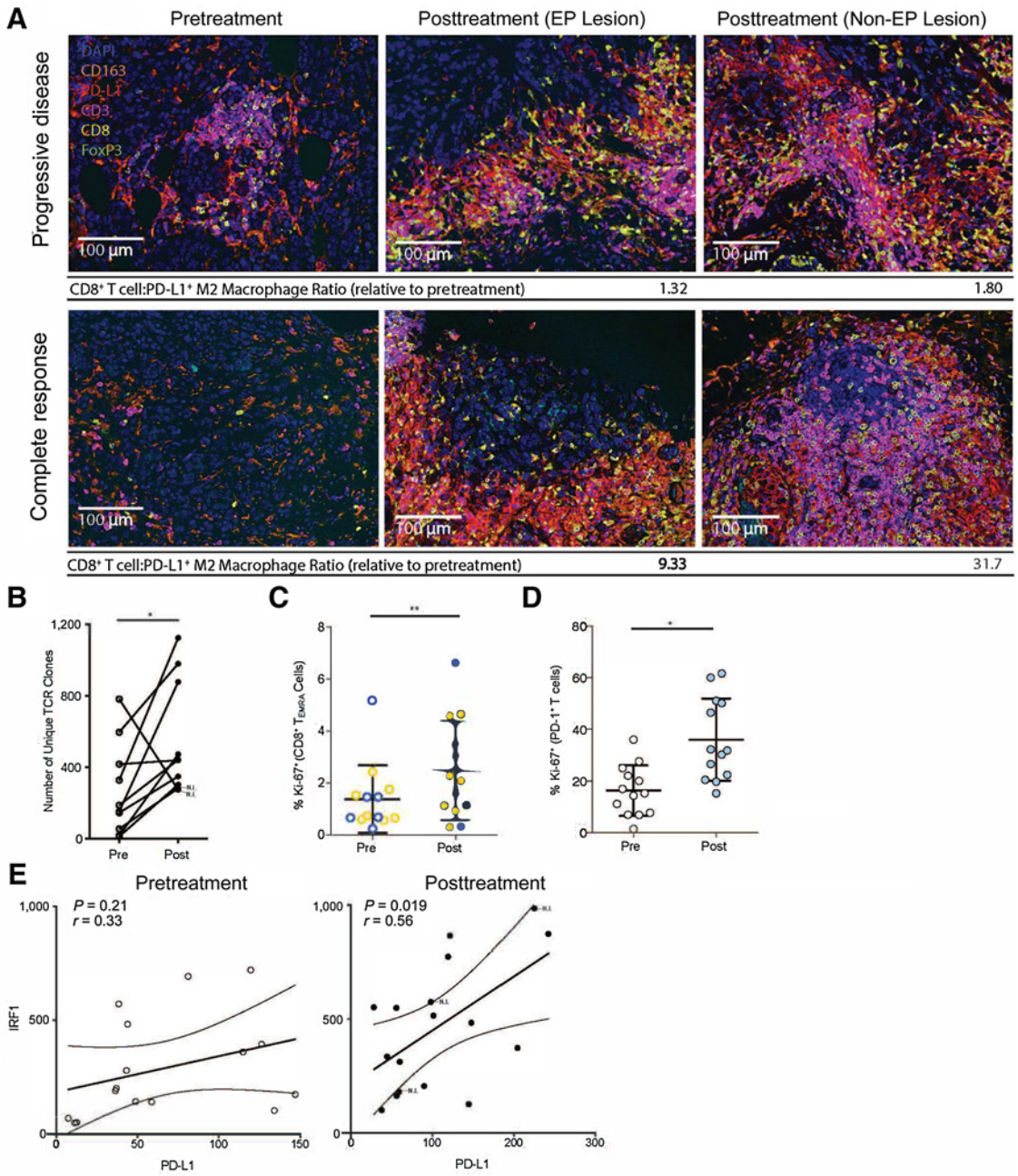

Figure 5.

Treatment-related increases in intratumoral CD8$^+$ T cell infiltration, adaptive resistance, and peripheral T cells. **A** An increase in lymphocyte infiltration was observed in both injected (EP) and noninjected (non-EP) tumors of patients regardless of response while the treatment-related ratio of CD8$^+$ T cells:CD163$^+$ M2 macrophages was increased in the responding patient. **B,** A significant increase was noted in unique intratumoral TCR clones emerging on treatment. **C** and **D,** Combination therapy resulted in a significantly increased percentage of proliferating CD8$^+$ effector memory RA$^+$ T cells and PD-1$^+$ T cells in the blood (PBMC) posttreatment. **E,** Transcriptional analysis demonstrated a significant increase in the treatment-related correlation between intratumoral IRF1 and PD-L1 expression. NR, nonresponder; R, responder; pre, pretreatment; post, posttreatment, cycle 2 day 1; EP lesion, injected and electroporated lesion; non-EP lesion, noninjected and nonelectroporated lesion. Significance calculated by Wilcoxon matched-pairs signed rank test $n = 10$ (**B**), $n = 13$ (**C** and **D**); Pearson correlation analysis with D'Agostino and Pearson normality test (**E**) $n = 16$ (pre), $n = 17$ (post; ns, not significant; *, $P < 0.05$; **, $P < 0.01$; N.I., noninjected lesions were noted (**B** and **E** only).

immunologically quiescent tumors have been lacking. Previously, we have demonstrated that immunologically relevant temporal intratumoral expression of IL-12 using gene electroporation can convert noninflamed to inflamed Th1-polarized tumors in animal models (24, 25).

Given these data, we administered i.t.-tavo-EP and pembrolizumab concurrently to patients determined to be unlikely to respond to anti-PD1 monotherapy based on a low frequency of cpCTL in the tumor microenvironment (26–31). Clinically, a

RECIST objective response rate of 41% was observed with 36% complete responses in this poorly inflamed, "cold" melanoma population with a predicted anti-PD-1 antibody response rate of < 12.5% based on the cpCTL assay and a low probability of response based on PDL-1 IHC (16) and IFNγ scores (17). Notably, 42% of patients had previously experienced disease progression on anti-PD-1 antibodies and the consistency between these clinical and immunologic negative predictors of response to anti-PD-1 antibodies suggests that the overall population was unlikely to respond. Our earlier work suggested that the duration of clinical responses to i.t.-tavo-EP monotherapy might be limited by the induction of adaptive resistance (13). In this study, analysis of serial biopsy specimens suggests substantial mechanistic interplay whereby pembrolizumab limits i.t.-tavo-EP–induced adaptive resistance, supporting the maintenance of the IL-12/IFNγ feedforward loop, which is fundamental for DC maturation and the resulting adaptive cellular responses. Reshaping of immunologically inert tumors was evident after 1 cycle of treatment with a global increase in immune-associated gene expression, including key transcripts associated with innate and adaptive immune responses. Specifically, we noted increases in antigen presenting cell (APC) and NK-cell–associated transcripts, inflammatory cytokines and chemokines, and genes related to adaptive cellular immunity including T cell activation, costimulation, and adaptive resistance. Marked ingress of $CD8^+$ T cells, measured by mIHC and emerging TCR clones, were all consistent with productive immune responses. This treatment-related change in the tumor microenvironment could be seen in both i.t.-tavo–EP injected and in uninjected tumors. When combined with the supportive peripheral NK and T cell phenotypic changes, these data collectively demonstrate promotion of a systemic anti-tumor immune response. The sustained, systemic effects of i.t.-tavo-EP in combination with pembrolizumab observed here are in contrast to previous studies of systemic IL-12, which induces objective responses in only 3–5% of patients and which is associated with high rates of severe side effects (9).

While the safety profile, clinical responses, and concordant translational data obtained in patients treated with i.t.-tavo-EP and pembrolizumab are highly encouraging in responding patients, further studies will be useful to understand mechanisms of resistance in nonresponding patients. In particular, the impact of differences in HLA variability, tumor antigenicity (32, 33), disregulation of WNT–β-catenin pathway (34, 35), PTEN loss (36), p53 loss (37), and deletional mutations in the JAK1/2–STAT (38) signaling pathway may influence responses to i.t.-tavo-EP. In addition, this study is limited to patients with superficial, accessible disease. While this current applicator can only treat tumors to a depth of 1.5 cm, a novel lesion applicator able to deliver plasmid to deep visceral organs is under development and could broaden the spectrum of treated tumors.

In summary, we show that i.t.-tavo-EP, combined with pembrolizumab in cpCTL poor melanoma can result in deep, durable, and frequent clinical responses, including responses in patients who have failed previous anti-PD-1 therapy. This approach may help to induce remissions in patients who are clinically refractory to anti-PD-1 therapies. A confirmatory trial to establish the therapeutic value of combining i.t.-tavo-EP and anti-PD-1 antibody therapy in anti-PD-1 relapsed/refractory patients with stage III/IV metastatic melanoma is currently underway with encouraging preliminary data to date.

Disclosure of Potential Conflicts of Interest

A.P. Algazi is a paid consultant for OncoSec Medical, Inc., Array, Regeneron, Valitor Biosciences, reports receiving other commercial research support from Acerta, BMS, Merck, AstraZeneca, Incyte, Tessa, OncoSec, Dynavax, Genentech, Sensei, Amgen, and Medimmune, holds ownership interest (including patents) in OncoSec Medical, Inc. and Valitor Biosciences, and is an advisory board member/unpaid consultant for Sensei and Merck. C.G. Twitty is an employee/paid consultant for and holds ownership interest (including patents) in Oncosec, K.K. Tsai reports receiving other commercial research support from Oncosec and Regeneron. M.H. Le is an employee/paid consultant for Oncosec Medical, Inc. R.H. Pierce is an employee/paid consultant for OncoSec Medical. E. Browning is an employee/paid consultant for and holds ownership interest (including patents) in OncoSec Medical, Inc. R. Hermiz, D.A. Canton and D. Bannovong are employees/paid consultants for OncoSec. C.B. Bifulco holds ownership interest (including patents) in PrimeVax, is an advisory board member/unpaid consultant for PrimeVax, HalioDx, and BMS, and is listed as an inventor on a United States patent application for an image processing system and method for displaying multiple images of a biological specimen. S. Bhatia is an employee/paid consultant for BMS, EMD Serono and Sanofi-Genzyme, and reports receiving commercial research grants from BMS, Merck, Oncosec, Nantkwest, Exicure, Novartis, Immune Design and EMD Serono. R.H. Andtbacka is an employee/paid consultant for Merck, Novartis, Amgen, Pfizer and Seven and Eight Biopharmaceuticals Inc., and holds ownership interest (including patents) in Seven and Eight Biopharmaceuticals Inc. B.A. Fox is an employee/paid consultant for Definiens/AstraZeneca, UltiVue and PerkinElmer, reports receiving commercial research grants from Akoya/PerkinElmer and OncoSec, and is an advisory board member/unpaid consultant for Akoya. M. Rosenblum is an employee/paid consultant for TRex Bio and Sitryx Bio. A.I. Daud reports commercial research funding from Merck, BMS, Roche, Pfizer, Incyte, and Novartis, ownership interest (including patents) in SQZ bio, Trex Bio, and OncoSec, and advisory/consultant relationships with Xencor, Checkmate, Incyte, Array, and Genentech. No potential conflicts of interest were disclosed by the other authors.

Authors' Contributions

Conception and design: A.P. Algazi, C.G. Twitty, M.H. Le, R.H. Pierce, S. Bhatia, R.H.I. Andtbacka, A.I. Daud

Development of methodology: A.P. Algazi, C.G. Twitty, R.H. Pierce, C. Ballesteros-Merino, S. Bhatia, B.A. Fox, A.I. Daud

Acquisition of data (provided animals, acquired and managed patients, provided facilities, etc.): A.P. Algazi, C.G. Twitty, K.K. Tsai, M.H. Le, R.H. Pierce, E. Browning, R. Hermiz, A. Oglesby, M. Francisco, C.B. Bifulco, C. Ballesteros-Merino, S. Bhatia, S. Gargosky, R.H.I. Andtbacka, B.A. Fox, M. Rosenblum, A.I. Daud

Analysis and interpretation of data (e.g., statistical analysis, biostatistics, computational analysis): A.P. Algazi, C.G. Twitty, R.H. Pierce, E. Browning, R. Hermiz, D.A. Canton, C.B. Bifulco, S. Bhatia, S. Gargosky, R.H.I. Andtbacka, B.A. Fox, M. Rosenblum, L. Fong, M.J. Pittet, S.P. Arlauckas, C. Garris, L. Levine, A.I. Daud

Writing, review, and/or revision of the manuscript: A.P. Algazi, C.G. Twitty, K.K. Tsai, E. Browning, R. Hermiz, D.A. Canton, D. Bannavong, C.B. Bifulco, S. Bhatia, S. Gargosky, R.H.I. Andtbacka, B.A. Fox, L. Fong, M.J. Pittet, S.P. Arlauckas, C. Garris, L. Levine, A.I. Daud

Administrative, technical, or material support (i.e., reporting or organizing data, constructing databases): A.P. Algazi, C.G. Twitty, K.K. Tsai, D. Bannavong, A. Oglesby, S. Gargosky, M. Rosenblum, A.I. Daud

Study supervision: A.P. Algazi, M.H. Le, S. Gargosky, R.H.I. Andtbacka, A.I. Daud

The costs of publication of this article were defrayed in part by the payment of page charges. This article must therefore be hereby marked *advertisement* in accordance with 18 U.S.C. Section 1734 solely to indicate this fact.

Received August 28, 2019; revised December 6, 2019; accepted March 20, 2020; published first May 6, 2020.

References

1. Kaliński P, Hilkens CM, Snijders A, Snijdewint FG, Kapsenberg ML. IL-12-deficient dendritic cells, generated in the presence of prostaglandin E2, promote type 2 cytokine production in maturing human naive T helper cells. J Immunol 1997;159:28–35.

2. Degliantoni G, Murphy M, Kobayashi M, Francis MK, Perussia B, Trinchieri G. Natural killer (NK) cell-derived hematopoietic colony-inhibiting activity and NK cytotoxic factor. Relationship with tumor necrosis factor and synergism with immune interferon. J Exp Med 1985;162:1512–30.
3. Hsieh CS, Macatonia SE, Tripp CS, Wolf SF, O'Garra A, Murphy KM. Development of TH1 CD4+ T cells through IL-12 produced by Listeria-induced macrophages. Science 1993;260:547–9.
4. Zhao J, Zhao J, Perlman S. Differential effects of IL-12 on tregs and non-treg T cells: roles of IFN-γ, IL-2 and IL-2R. PLoS One 2012;7:e46241.
5. Kerkar SP, Goldszmid RS, Muranski P, Chinnasamy D, Yu Z, Reger RN, et al. IL-12 triggers a programmatic change in dysfunctional myeloid-derived cells within mouse tumors. J Clin Invest 2011;121:4746–57.
6. Colombo MP, Trinchieri G. Interleukin-12 in anti-tumor immunity and immunotherapy. Cytokine Growth Factor Rev 2002;13:155–68.
7. Bashyam H. Interleukin-12: a master regulator. J Exp Med 2007;204:969.
8. Garris CS, Arlauckas SP, Kohler RH, Trefny MP, Garren S, Piot C, et al. Successful Anti-PD-1 Cancer Immunotherapy Requires T Cell-Dendritic Cell Crosstalk Involving the Cytokines IFN-γ and IL-12. Immunity 2018;49:1148–61.
9. Atkins MB, Robertson MJ, Gordon M, Lotze MT, DeCoste M, DuBois JS, et al. Phase I evaluation of intravenous recombinant human interleukin 12 in patients with advanced malignancies. Clin Cancer Res 1997;3:409–17.
10. Del Vecchio M, Bajetta E, Canova S, Lotze MT, Wesa A, Parmiani G, et al. Interleukin-12: biological properties and clinical application. Clin Cancer Res 2007;13:4677–85.
11. Heller L, Merkler K, Westover J, Cruz Y, Coppola D, Benson K, et al. Evaluation of toxicity following electrically mediated interleukin-12 gene delivery in a B16 mouse melanoma model. Clin Cancer Res 2006;12:3177–83.
12. Daud AI, DeConti RC, Andrews S, Urbas P, Riker AI, Sondak VK, et al. Phase I trial of interleukin-12 plasmid electroporation in patients with metastatic melanoma. J Clin Oncol 2008;26:5896–903.
13. Algazi A, Bhatia S, Agarwala S, Molina M, Lewis K, Faries M, et al. Intratumoral delivery of tavokinogene telseplasmid yields systemic immune responses in metastatic melanoma patients. Ann Oncol 2020;31:532–40.
14. Daud AI, Loo K, Pauli ML, Sanchez-Rodriguez R, Sandoval PM, Taravati K, et al. Tumor immune profiling predicts response to anti-PD-1 therapy in human melanoma. J Clin Invest 2016;126:3447–52.
15. Loo K, Tsai KK, Mahuron K, Liu J, Pauli ML, et al. Partially exhausted tumor-infiltrating lymphocytes predict response to combination immunotherapy. JCI Insight 2017;20;2(14):e93433.
16. Daud AI, Wolchok JD, Robert C, Hwu WJ, Weber JS, Ribas A, et al. Programmed death-ligand 1 expression and response to the anti-programmed death 1 antibody pembrolizumab in melanoma. J Clin Oncol 2016;34:4102–9.
17. Ayers M, Lunceford J, Nebozhyn M, Murphy E, Loboda A, Kaufman DR, et al. IFN-γ-related mRNA profile predicts clinical response to PD-1 blockade. J Clin Invest 2017;127:2930–40.
18. Tumeh PC, Harview CL, Yearley JH, Shintaku IP, Taylor EJ, Robert L, et al. PD-1 blockade induces responses by inhibiting adaptive immune resistance. Nature 2014;515:568–71.
19. Pagès F, Kirilovsky A, Mlecnik B, Asslaber M, Tosolini M, Bindea G, et al. In situ cytotoxic and memory T cells predict outcome in patients with early-stage colorectal cancer. J Clin Oncol 2009;27:5944–51.
20. Spranger S, Sivan A, Corrales L, Gajewski TF. Tumor and host factors controlling antitumor immunity and efficacy of cancer immunotherapy. Adv Immunol 2016;130:75–93.
21. Smithy JW, Moore LM, Pelekanou V, Rehman J, Gaule P, Wong PF, et al. Nuclear IRF-1 expression as a mechanism to assess "Capability" to express PD-L1 and response to PD-1 therapy in metastatic melanoma. J Immunother Cancer 2017;5:25.
22. Vignali DA, Kuchroo VK. IL-12 Family Cytokine: Immunological playmakers. Nature Immunol 2012;13:722–8.
23. Lucey DR, Clerici M, Shearer GM. Type 1 and type 2 cytokine dysregulation in human infectious, neoplastic, and inflammatory diseases. Clin Microbiol Rev 1996;9:532–62.
24. Lucas ML, Heller R. IL-12 gene therapy using an electrically mediated nonviral approach reduces metastatic growth of melanoma. DNA Cell Biol 63–22:755;2003.
25. Heller LC, Heller R. In vivo electroporation for gene therapy. Hum Gene Ther 2006;17:890–7.
26. Duhen T, Duhen R, Montler R, Moses J, Moudgil T, de Miranda NF, et al. Co-expression of CD39 and CD103 identifies tumor-reactive CD8 T cells in human solid tumors. Nat Commun 2018;9:2724.
27. Gros A, Robbins PF, Yao X, Li YF, Turcotte S, Tran E, et al. PD-1 identifies the patient-specific CD8+ tumor-reactive repertoire infiltrating human tumors. J Clin Invest 2014;124:2246–59.
28. Huang AC, Postow MA, Orlowski RJ, Mick R, Bengsch B, Manne S, et al. T-cell invigoration to tumour burden ratio associated with anti-PD-1 response. Nature 2017;545:60–5.
29. Li H, van der Leun AM, Yofe I, Lubling Y, Gelbard-Solodkin D, van Akkooi ACJ, et al. Dysfunctional CD8 T cells form a proliferative, dynamically regulated compartment within human melanoma. Cell 2019;176:775–89.
30. Simoni Y, Becht E, Fehlings M, Loh CY, Koo SL, Teng KWW, et al. Bystander CD8+ T cells are abundant and phenotypically distinct in human tumour infiltrates. Nature 2018;557:575–9.
31. Thommen DS, Koelzer VH, Herzig P, Roller A, Trefny M, Dimeloe S, et al. A transcriptionally and functionally distinct PD-1+ CD8+ T cell pool with predictive potential in non-small-cell lung cancer treated with PD-1 blockade. Nat Med 2018;24:994–1004.
32. Rizvi NA, Hellmann MD, Snyder A, Kvistborg P, Makarov V, Havel JJ, et al. Cancer immunology. mutational landscape determines sensitivity to PD-1 blockade in non-small cell lung cancer. Science 2015;348:124–8.
33. Verdegaal EME, de Miranda NFCC, Visser M, Harryvan T, van Buuren MM, Andersen RS, et al. Neoantigen landscape dynamics during human melanoma-T cell interactions. Nature 2016;536:91–5.
34. Luke JJ, Bao R, Sweis RF, Spranger S, Gajewski TF. WNT/β-catenin pathway activation correlates with immune exclusion across human cancers. Clin Cancer Res 2019;25:3074–83.
35. Spranger S, Bao R, Gajewski TF. Melanoma-intrinsic β-catenin signalling prevents anti-tumour immunity. Nature 2015;523:231–5.
36. Brandmaier A, Hou S-Q, Demaria S, Formenti SC, Shen WH. PTEN at the interface of immune tolerance and tumor suppression. Front Biol 2017;12:163–74.
37. Muñoz-Fontela C, Mandinova A, Aaronson SA, Lee SW. Emerging roles of p53 and other tumour-suppressor genes in immune regulation. Nat Rev Immunol 2016;16:741–50.
38. Shin DS, Zaretsky JM, Escuin-Ordinas H, Garcia-Diaz A, Hu-Lieskovan S, Kalbasi A, et al. Primary resistance to PD-1 blockade mediated by JAK1/2 mutations. Cancer Discov 2017;7:188–201.

AACR American Association for Cancer Research

Clinical Cancer Research

Phase II Trial of IL-12 Plasmid Transfection and PD-1 Blockade in Immunologically Quiescent Melanoma

Alain P. Algazi, Christopher G. Twitty, Katy K. Tsai, et al.

Clin Cancer Res Published OnlineFirst May 6, 2020.